AD-A050 021 NAVAL POSTGRADUATE SCHOOL MONTEREY CALIF F/G 20/1
SOUND TRANSMISSION FROM A TAPERED FLUID LAYER INTO A FAST BOTTO--ETC(U)
DEC 77 G B NETZORG

UNCLASSIFIED NL

1 OF 1
AD A050021

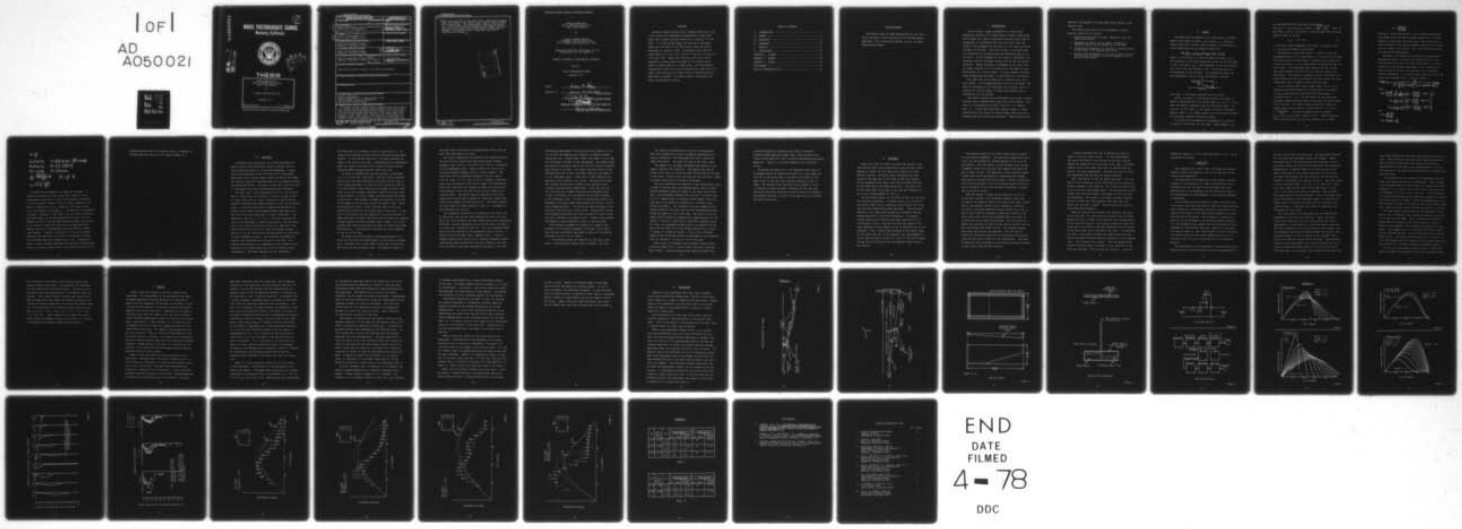

END
DATE FILMED
4-78
DDC

NAVAL POSTGRADUATE SCHOOL
Monterey, California

THESIS

SOUND TRANSMISSION
FROM A TAPERED FLUID LAYER
INTO A FAST BOTTOM

by

Gregory Bertman Netzorg

December 1977

Thesis Advisor: J. V. Sanders

UNCLASSIFIED

SECURITY CLASSIFICATION OF THIS PAGE (When Data Entered)

REPORT DOCUMENTATION PAGE

READ INSTRUCTIONS BEFORE COMPLETING FORM

1. REPORT NUMBER

2. GOVT ACCESSION NO.

3. RECIPIENT'S CATALOG NUMBER

4. TITLE (and Subtitle)

Sound Transmission from a Tapered Fluid Layer into a Fast Bottom,

5. TYPE OF REPORT & PERIOD COVERED

Master's Thesis;
December 1977

6. PERFORMING ORG. REPORT NUMBER

7. AUTHOR(s)

Gregory Bertman Netzorg

8. CONTRACT OR GRANT NUMBER(s)

9. PERFORMING ORGANIZATION NAME AND ADDRESS

Naval Postgraduate School
Monterey, California 93940

10. PROGRAM ELEMENT, PROJECT, TASK AREA & WORK UNIT NUMBERS

11. CONTROLLING OFFICE NAME AND ADDRESS

Naval Postgraduate School
Monterey, California 93940

12. REPORT DATE

December 1977

13. NUMBER OF PAGES

14. MONITORING AGENCY NAME & ADDRESS(if different from Controlling Office)

Naval Postgraduate School
Monterey, California 93940

48 p.

15. SECURITY CLASS. (of this report)

Unclassified

15a. DECLASSIFICATION/DOWNGRADING SCHEDULE

16. DISTRIBUTION STATEMENT (of this Report)

Approved for public release; distribution unlimited.

17. DISTRIBUTION STATEMENT (of the abstract entered in Block 20, if different from Report)

18. SUPPLEMENTARY NOTES

19. KEY WORDS (Continue on reverse side if necessary and identify by block number)

Acoustic waveguide
Sound Propagation in a Tapered Fluid Layer
Shallow Water Acoustic Propagation
Two-Layered Acoustic Model

20. ABSTRACT (Continue on reverse side if necessary and identify by block number)

Acoustic energy transfer from a tapered fluid layer into a fast bottom was investigated experimentally using fresh water and a saline solution separated by a sheet of 0.5 mil mylar. A 150 kHz pulsed signal was excited in the upper layer and a receiver in the lower fluid layer was used to determine the acoustic field. Measurements were made for taper angles of 1.52°, 2.51°, and 4.41° and for ρc ratios of 0.745 and 0.836.

DD FORM 1 JAN 73 1473 (Page 1)

EDITION OF 1 NOV 65 IS OBSOLETE
S/N 0102-014-6601

UNCLASSIFIED

SECURITY CLASSIFICATION OF THIS PAGE (When Data Entered)

251450

Beams were observed in the lower layer, beginning at points where the depth of the tapered layer equals a cutoff depth for a normal mode. The experimental beam patterns agree well with the theoretical predictions for angles from grazing to the angle where the maximum pressure amplitude is reached. For greater angles, experiment and theory significantly diverge.

Approved for public release; distribution unlimited.

Sound Transmission from a Tapered Fluid Layer into a Fast Bottom

by

Gregory Bertman Netzorg
Lieutenant, United States Navy
B.S., Oregon State University, 1970

Submitted in partial fulfillment of the
requirements for the degree of

MASTER OF SCIENCE IN ENGINEERING ACOUSTICS

from the

NAVAL POSTGRADUATE SCHOOL

December 1977

Author Gregory B. Netzorg

Approved by: James V. Sanders
Thesis Advisor

Allan B. Coppens
Second Reader

R. E. Walker
Chairman, Department of Physics and Chemistry

George J. Haltiner
Dean of Science and Engineering

ABSTRACT

Acoustic energy transfer from a tapered fluid layer into a fast bottom was investigated experimentally using fresh water and a saline solution separated by a sheet of 0.5 mil mylar. A 150 kHz pulsed signal was excited in the upper layer and a receiver in the lower fluid layer was used to determine the acoustic field. Measurements were made for taper angles of 1.52°, 2.51°, and 4.41° and for ρc ratios of 0.745 and 0.836. Beams were observed in the lower layer, beginning at points where the depth of the tapered layer equals a cutoff depth for a normal mode. The experimental beam patterns agree well with the theoretical predictions for angles from grazing to the angle where the maximum pressure amplitude is reached. For greater angles, experiment and theory significantly diverge.

TABLE OF CONTENTS

I. INTRODUCTION---------- 7

II. THEORY---------- 9

III. APPARATUS---------- 14

IV. PROCEDURE---------- 20

V. RESULTS---------- 27

VI. CONCLUSIONS---------- 32

APPENDIX A: FIGURES---------- 33

APPENDIX B: GRAPHS---------- 38

APPENDIX C: TABLES---------- 46

BIBLIOGRAPHY---------- 47

INITIAL DISTRIBUTION LIST---------- 48

ACKNOWLEDGEMENT

The author wishes to thank Bob Moeller for his technical assistance in the construction of the experimental apparatus. This research was funded, in part, by Naval Ocean Systems Center.

I. INTRODUCTION

For an acoustic signal propagated in a fluid layer overlying a bottom with a higher speed of sound, normal mode theory shows that energy associated with each normal mode of propagation is transferred from the fluid layer into the bottom if the frequency of the source is less than the cutoff frequency of the mode. This can be seen if the normal mode is represented by an upward-going and downward-going ray in the layer. As the frequency of the signal is decreased, the (grazing) angle of incidence between the ray and the bottom increases. Energy continues to propagate in the layer with no energy transfer into the bottom, until the angle of incidence equals the critical angle. At that frequency the mode stops propagating and energy is transferred into the bottom.

This same idea can be applied to a tapered layer over a fast bottom. As a propagating mode travels up the wedge, the angle of incidence of the equivalent ray increases until it reaches the critical angle, at which point energy will be transmitted into the bottom.

This thesis reports on an investigation of acoustic energy transfer from a tapered fluid layer into a fast bottom. This work is a continuation of a thesis done by J. N. Edwards [Ref. 1]. It had been found that acoustic energy is transmitted into a fast bottom in beams through finite apertures located along the fluid-fluid interface. The position of the

apertures corresponded to normal mode cutoff depths in the tapered layer.

The primary objectives of the experimental research reported herein are as follows:

1. Confirm the existence of beams transmitted into the lower fluid layer.
2. Determine the effect of the source transducer's radiation pattern on the properties of the beam.
3. Determine the dependence of the beam's characteristics on the slope of the tapered fluid layer.
4. Determine the dependence of the beam's characteristics on the ratios of specific acoustic impedance, ρc, of the two fluid layers.

II. THEORY

One-dimensional propagation in a fluid layer of uniform depth H with speed of sound c_1 and density ρ_1, overlying a second layer with a faster speed of sound, c_2 and density ρ_2, can be represented by an equation of the form

$$P = \sum_n A_n \sin(k_{zn} z) \exp i(\omega t - k_{xn} x)$$

where z is the depth, x is the horizontal distance, k_{zn} is the component of the wave propagation vector for the nth mode in the z direction, k_{xn} is the component of the wave propagation vector for the nth mode in the x direction, and A_n is the magnitude of the nth mode. For propagating modes, the wave propagation vector can be represented as follows:

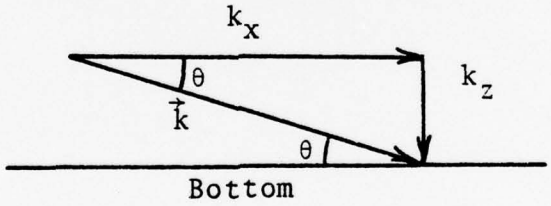

Note that θ is the angle between $\vec{k}$ and the bottom.

Snell's Law gives a relationship between the speeds of sound in the layers and the critical angle θ_c, $\cos\theta_c = c_1/c_2$, where the angle is measured from the horizontal plane. As long as θ is less than θ_c, the energy is totally reflected. However, when $\theta = \theta_c$, energy begins to be transmitted through the previously totally reflecting surface.

To satisfy the requirements of propagation, k_{zn} must be a constant, real number for each mode. These numbers, k_{zn},

are obtained from the following relationship:
$\tan k_{zn} H = -(\rho_2/\rho_1)(k_{zn}/\gamma_n)$ where $\gamma_n = \sqrt{k_x^2 - (\frac{\omega}{c_2})^2}$ [Ref. 2]. Once the ρ's and c's are given, it can be shown from the above equation that, at cutoff,

$$k_{zn} H = (n - 1/2)\pi \qquad (1)$$

so that for a mode propagating just above its cutoff, there is a pressure antinode at the bottom.

Now consider a wedge with angle β. Figure 1 shows the propagating vector of a single mode as it travels down a wedge. With each bounce off the bottom, θ increases by an amount 2β. At the point where $\theta = \theta_c$, energy begins to penetrate into the lower layer. The remaining energy bounces off the top and then makes another collision with the bottom, losing still more energy. This process continues until all the energy has been transferred into the bottom or the wave reaches the turn-around point and is reflected back into the wedge.

In the constant depth case, higher modes are cut off as frequency decreases because $\vec{k}$ is proportional to frequency; with k_{zn} being fixed for each mode and $\vec{k}$ decreasing, θ increases until $\theta = \theta_c$. For the wedge, on the other hand, frequency remains constant while θ increases with each bounce off the bottom. The depth at which cutoff for a mode in a wedge occurs can be found by solving equation (1) for H ; $H = \frac{(n - 1/2)\pi}{k_{zn}}$. From the propagating vector diagram, $k_{zn} = k \sin \theta_c$ at cutoff, where $k \equiv 2\pi/\lambda$. Substituting the above expression for k_{zn} into the equation for H yields:

$$H_o = \frac{(n-\frac{1}{2})\,\lambda}{2 \sin \theta_c}$$

Knowing H_o allows calculation of the location where energy will begin transiting the interface between the two layers. Dumping of energy into the lower layer takes place over a finite distance. This finite aperture results in the formation of a beam in the bottom. Thus, the characteristics of the beam can be approximated.

Professor A. B. Coppens has formulated an approximate mathematical model to predict the characteristics of the transmitted beam in the fast-fluid layer [Ref. 3]. The expression for the pressure amplitude, R, as a function of angle of depression from the interface, θ, is presented without explanation. X is the distance from the apex to the point where dumping starts. Refer to figure 2.

$$R(\theta) = \frac{1}{2}\, u\, \frac{e^{G}}{\sqrt{1-\frac{x_o'}{X}}\left[B'^2+4A'D'\right]^{1/4}\left[1-2\cos\theta\,\frac{x_o'}{r}+\left(\frac{x_o'}{r}\right)^2\right]^{3/4}}$$

Where

$$G = \frac{\tan\theta_c}{\tan\beta}\,\frac{b^2}{b^2-1}\,\frac{c}{\sqrt{b^2-c^2}}\left[\sin^{-1}\frac{c^2+bz}{c(b+z)} - \sin^{-1}\frac{c}{b}\right]$$
$$- \frac{1}{2}\,\frac{1}{\tan\beta}\,\frac{1}{b-1}\left[\sin^{-1}\frac{c^2+z}{c(1+z)} - \sin^{-1} c\right]$$
$$+ \frac{1}{2}\,\frac{1}{\tan\beta}\,\frac{1}{b+1}\left[\sin^{-1}\frac{c^2-z}{c(1-z)} - \sin^{-1} c\right]$$

and

$$u = \frac{\sin\theta}{\tan\theta_c}$$

$$c = \cos\theta_c = \frac{c_1}{c_2}$$

$$b = \frac{\rho_2}{\rho_1}$$

$$A = A' \tan^2 \theta_c \qquad A' = \frac{3}{2}\left[3 + \tan^2 \theta_c - \left(\frac{X}{r}\right) u^2 \cos \Theta\right]$$

$$B = B' \tan^2 \theta_c \qquad B' = 2\left[1 - \frac{1}{2}\left(\frac{X}{r}\right) u^2\right]$$

$$D = 1 - \cos \Theta \qquad D' = D / \tan^2 \theta_c$$

$$\frac{X_o'}{X} = \frac{\sqrt{B^2 + 4AD} - B}{2A} \qquad \frac{X_o'}{r} = \frac{X_o'}{X} \frac{X}{r}$$

$$Z = \sqrt{1 - \left(1 - \frac{X_o'}{X}\right)^2}$$

The model was programmed on a WANG 2200 computer. A sensitivity analysis was run using input values to match experimental conditions in order to investigate the effects of four variables; changes in the X/r ratio, changes in the speed of sound ratio, c_1/c_2, changes in the density ratio, ρ_2/ρ_1, and changes in the angle β. The analyses are presented on graphs 1 through 4. Note that as the X/r ratio increases, the beam widens, the maximum amplitude decreases, but the angular position of the maximum amplitude changes very little. As the speed of sound ratio decreases, maximum amplitude, angular position of the maximum, and beam width all change significantly. Changes in the density ratio alter maximum amplitude and beam width very little; the angular position of the maximum amplitude changed quite a bit. Changing the angle β, alters maximum amplitude and beam width significantly; there is an almost linear shift in the angular position of the

maximum amplitude with an average of about 1.5 degrees of maximum amplitude shift per 0.01 degree change in β.

III. APPARATUS

Experiments were carried out in a tank consisting of a wedge of fresh water overlying a saline solution; the two fluids being kept apart by a thin mylar membrane. A sound source was positioned at the thick end of the fresh-water wedge which sent a pulsed signal toward the apex of the wedge. The tank was lined with absorbing material to eliminate reflections from the bottom. A receiver in the lower fluid was used to investigate the sound field penetrating the interface.

The tank (Fig. 3) was constructed of 0.5 in. thick lucite sheet. Overall size of the tank is 14-1/8 in. wide, 10-5/16 in. high, and 30-3/8 in. long. A portion of the bottom was slanted to decrease the required amount of fluid in the bottom layer. A one-inch thick layer of rubberized horsehair was placed on the bottom, up the angled bottom, and against the left end of the tank (deep end) to reduce reflections. Two reflectors, about 11 in. by 2.5 in., were also utilized for part of the experiment to reduce interference. They were made from 0.5 in. thick lucite with a 0.0625 in. deep cavity cut into one face, with a 0.125 in. wide rim around the edge. A piece of 0.125 in. thick lucite was then glued over the cavity to form a trapped air space. One reflector was mounted on brackets that were hung over the side of the tank. This allowed the reflector to be suspended at any location in the tank and to be rotated about the y-axis to minimize signal interference. The other reflector was not adjustable.

The frame had to be removed in order to reposition it. All seams of the tank were joined with Dow Corning Silicone Rubber Sealant. A clear plastic grid with 1 cm-square markings was taped to the front of the tank. A matching grid on translucent paper was taped to the back of the tank so paralax could be minimized when locating positions inside the tank.

In order to separate the two fluid layers, a frame made of 0.5 in. lucite was constructed. Half-mil thick, aluminum coated mylar was then fastened to the bottom of the frame by first taping one edge of a sheet of mylar, metalized side up, to a flat surface, then stretching and taping the other three sides to the flat surface, applying a bead of silicone rubber to the bottom of the lucite frame, and then placing the frame on the mylar. Fifty pounds of weight were applied to the top of the frame for twelve hours while the sealant cured. After the sealant was cured, a razor blade was used to trim the excess mylar flush with the outside edge of the frame. A thin coat of the sealant was then applied to the outside mylar-to-frame interface to prevent the brine from attacking the aluminum coating causing the mylar-to-frame seal to erode. Two lucite spreader bars were used between the sides to prevent the frame from bowing in. This tray-like structure was then suspended in the top of the tank.

The brine solution was made by mixing approximately 41 liters of tap water with approximately 15 kg of water softener salt. Tap water with several drops of red food coloring was the fluid used for the upper layer. The amount of water in

the upper layer varied with the experimental set-up, but was never more than about two liters.

Two source transducers were made for the research project. The first one was constructed from three barium titanate elements, each 0.125 in. by 0.125 in. by 0.200 in., polarized in the longitudinal mode. Contact cement was used to join the three elements together and to a lucite support. The active face of the transducer measured 0.125 in. high by 0.375 in. long. A 6 in. long, 0.250 in. diameter, stainless steel tube was mounted to the lucite support with epoxy glue. Electrical leads were run through the tube with the positive lead fastened to the rear face of the barium titanate with silvered epoxy. The ground lead was epoxied to the lucite support with silver paint, making the electrical connections between the elements and the ground wire. The whole assembly was then dipped in liquid neoprene to seal it. Resonance of the transducer was 416 kHz.

The transducer worked well, but because of the small area of the active face and the high frequency at which the transducer had to be operated, too many normal modes were propagating. Therefore, a mylar transducer with an active face, 2 cm high by 8 cm wide, was constructed (Fig. 4). The 1 mil aluminum coated mylar face was attached to the transducer body as follows: A protective mask was made from a computer card. It was cut slightly smaller than the 8 cm by 2 cm metal transducer insert. Then masking tape was placed on the mask, adhesive side down, with the edges of the tape overlapping the edges of the mask.

The masking tape/computer card mask was then trimmed to 2 cm by 8 cm with the masking tape acting as an adhesive border around the card. Another mask, about 1 mm larger in size than the first mask, was made in the same manner. The smaller mask was placed on the metal insert with the thin strips of masking tape holding it in place. The larger mask was placed on the non-metalized side of the 1 mil mylar which was stretched in a 5 in. embroidery hoop. A thin coat of spray adhesive was applied to both surfaces to be joined. The protective masks were removed and the mylar joined to the transducer body, lining up the previously masked areas. After the glue was dry, the mylar was trimmed flush with the transducer body. A layer of aluminum foil was epoxied to the other surfaces of the transducer body. In order to electrically shield the transducer, all outer seams were painted with silver, electrically conducting paint. The shield was then continued to the stainless steel tube with silver paint. The positive lead of the transducer had previously been run down the inside of the tube and connected to the metal insert. Finally, the assembly was dipped in liquid neoprene to seal it from the water.

The transducer assembly was mounted on a support that allowed it to be located anywhere in the upper fluid layer. Fine vertical adjustments were made by means of a micrometer adjustment with 1/2 in. of travel.

A dc biasing-voltage was required for the mylar transducer. The electrical network shown in figure 5 was used.

Two receiver hydrophones were used in the experiment. Both were standard LC5-2 probe transducers manufactured by Celesco Industries. One hydrophone was used to probe the upper fluid layer. The other was used in the lower layer.

The support for the upper hydrophone was similar to the support used for the transducer. The support was able to slide on the sides of the mylar frame from one end of the tank to the other. Travel across the tank was also possible. Depth was again varied with a micrometer adjustment.

The lower hydrophone was mounted so that measurements could be made at varying radii and changing angles about a center located somewhere along the length of the fluid-fluid interface. The hydrophone extended from the end of the short leg of an "L" shaped piece of stainless steel tubing, while the long leg of the tubing was attached to a circular, clear plastic protractor. The protractor was then clamped to the inside surface of the tank side with the hydrophone pointing toward the opposite side of the tank. The radius of the arc swung could be varied by changing the clamped position of the tubing. In order to take data at different distances across the tank, the hydrophone assembly had to be removed from the water and the short leg of the tubing replaced with a piece of tubing of a different length. A set of five different length pieces of tubing allowed the hydrophone to be supported from the centerline to the far side of the tank.

Other pieces of equipment used included a General Radio Oscillator model 1310, a General Radio Tone Burst Generator model 1396-A, a Hewlett-Packard Power Amplifier model 467A,

a Hewlett-Packard ac Voltmeter model 400D, two Hewlett-Packard Voltage Amplifiers model 465A, a SKL Variable Electronic Filter model 302, and a Tectronix Dual-Beam Oscilloscope model 565. Figure 6 is a block diagram of the electrical set-up.

To measure the angle β, a C. W. Radiation Laser with 0.5 mW maximum output was mounted vertically on a ring stand with the face of the laser about 30 cm above the surface of the upper layer so that the laser beam was parallel to the y-z plane. The bottom of the laser was tilted slightly in the -y direction so that the beam reflected off the top layer would miss the laser, itself, and strike a meter stick mounted horizontally and just in front of the laser about 30 cm above the face of the laser.

IV. PROCEDURE

Before any data was taken, the frame was placed in the tank and the water levels equalized so that the point where dumping of energy into the lower layer begins is at the desired location. The mylar source transducer was then placed in the deep end of the frame so that the surfaces of the transducer were about 2 mm from the bottom and back of the frame and on the frame centerline. The probe used in the lower layer was placed in the tank and connected to one of the voltage amplifiers (Fig. 6).

The oscillator output, set at about 150 kHz, was fed into the tone burst generator. A pulsed signal of 16 cycles of the 150 kHz input with a repetition rate of about 400 Hz was fed into the variable-gain power amplifier. From the power amplifier, the signal went through the transducer biasing network and then to the source transducer. An external trigger lead was run from the tone burst generator to the oscilloscope. Also, a lead was run from the output of the power amplifier to one channel of the oscilloscope and to the voltmeter. This allowed visual checking of the input signal to the source and, for set-up purposes only, measurement of the ac input voltage of about 18.3 volts to the source (meter voltage could be read only with an unpulsed signal going to the source).

The acoustic signal in the lower fluid layer was sensed by the receiver hydrophone. The electrical signal from the receiver was fed through two voltage amplifiers set at 40 dB gain apiece. Then the signal, with 80 dB gain, went through a bandpass filter with the pass band ranging from about 136 kHz to about 210 kHz. The amplitude of the received, pulsed signal could now be determined by integrating the average peak value by eye from the oscilloscope. Eyeball integration from the oscilloscope is not very accurate because often the top of the pulse is not flat and small differences in amplitude are hard to detect.

When the speeds of sound and the densities of the two fluids were required, the following procedures were used. To measure the speed of sound in the upper fluid layer (fresh water), the barium titanate source transducer, connected directly to the power amplifier output (dotted line, Fig. 6), and an LC5-2 receiver transducer connected in place of the lower layer probe, were each suspended from ring stands in the deep end of the water-filled frame. The oscillator frequency was increased to about 416 kHz and the filter reset to pass everything above about 200 kHz. The distance between the source and receiver was measured. Then the time of transit for the direct path of a 16-cycle pulse was measured using the time delay feature of the oscilloscope. The speed of sound was then calculated by dividing the measured distance by the transit time for that distance.

A similar procedure was used to measure the speed of sound in the lower layer (brine). For this measurement, the source and receiver were placed in the brine solution between the frame and the close side of the tank. The probe normally used in the lower layer must be removed from the tank for the above measurement. Distance and time of travel were determined and the speed of sound calculated.

Next, the density of the two fluids was found. This was done by first weighing a 60 ml, ASTM vessel on an analytical balance readable to one-tenth mg. The vessel was then filled to the 60 ml mark and weighed again. By subtracting the first weight from the second weight, the weight of 60 ml of water was determined. The weight of the water in grams divided by the 60 ml volume and, the quotient times 1000, gave the density of the water in kg/m^3. This procedure was done for both fluids when required.

When the slope of the interface was required, the laser set-up was used. The laser beam was directed into the water parallel to the y-z plane at the location where determination of the slope was desired. The beam was projected toward the close side of the tank so that the reflection off the surface of the water would not be blocked by the laser. To determine the slope, the distance between the surface-reflected beam and the interface-reflected beam was measured on the suspended ruler. This distance was called P. Then the perpendicular distance from the point of interest on the interface to the ruler was measured. This distance was called Q. Using the

refractive index of 1.33 for water and Snell's law, β can be calculated as follows:

$$\beta = \frac{\tan^{-1} P/Q}{2(1.33)}$$

Upon completion of a day's work, the frame was drained, removed, rinsed, and hung up to dry as was the rest of the brine-covered apparatus.

The experiment was carried out in four phases: re-establishment of the existence of a beam, determination of the characteristics of the beam in the horizontal direction, determination of the dependence of the beam on the angle β, and determination of the dependence of the beam on changing ρc mismatches.

To re-establish the existence of a beam, the probe used in the lower layer was positioned to take data along vertical lines located at 5 cm intervals along the centerline of the tank with the origin of the beam occurring about 43 cm from the deep end of the frame. Peak voltages of a pulse were read off the oscilloscope as the probe was moved vertically in 5 mm increments which ranged from the surface/mylar-brine interface to the bottom of the tank. Results of this phase are shown on graph 5. Note that distances in the x-direction are measured from the point where dumping begins (Fig. 2); distances from this point toward the apex are considered positive.

The second phase of the experiment, determining the beam's characteristics in the horizontal direction, perpendicular to

the axis of the beam, was done next. The measuring technique for this phase and subsequent phases was changed. Rather than measuring in the vertical plane and plotting in an x-y coordinate system, the probe was rotated about the calculated dumping point, located at about 33 cm from the end of the frame's deep end, so that polar coordinates could be used. The radii and distances off the centerline of the tank were changed to investigate the areas of interest. Data were taken at three different radii: 10.3 cm, 15 cm, and 20 cm. These arcs were swung with the probe on the centerline, 2.5 cm, 5 cm, 7.5 cm, and 10 cm off the centerline. Peak voltages were again read off the oscilloscope. Plots of voltage versus angle (referenced to the horizontal plane) for the three different radii at different distances off the centerline are shown in graph 6. Densities and speeds of sound were also determined for this phase.

The third phase of the experiment was to determine the dependence of the beam on the angle β. Again, the water levels were equalized at a level that allowed the initial dumping point to fall about 33 cm from the frame's deep end. The lucite reflectors were also inserted at this stage. The non-suspended reflector was placed between two pieces of rubberized horsehair so that it rested on the slanted bottom about 28 cm from the shallow end of the tank. The suspended reflector was placed about 30 cm from the shallow end of the tank at a depth that would allow it to clear the bottom of the frame when it was rotated. More rubberized horsehair was

also added between the reflectors and the shallow end of the tank. These reflectors and additional rubberized horsehair were installed to help block the second mode which was transmitted into the lower layer starting about 12 cm from the deep end of the frame and interfering with the beam from the first mode.

The procedure for this phase of the experiment was basically the same as that for the second phase. Peak voltages were determined from the oscilloscope as a function of θ at different r's: 10.3 cm, 15 cm, 20 cm, 25 cm, and 30 cm, and at different β's: 1.52°, 2.51°, and 4.41°. β was decreased by raising the deep end of the frame and increased by raising the shallow end of the frame. The initial dumping point was held constant at about 33 cm from the end of the frame's deep end. Results of this phase are shown on graphs 7, 8, and 9.

The final phase, determination of the dependence of the beam on the ρc mismatch, used the same coordinate system and r's as the previous phase. The ρc mismatch was altered by decreasing the salinity of the brine solution. About 18 liters of the original brine solution were replaced with tap water. This changed the ρ of the brine from 1146.97 kg/m^3 to 1087.42 kg/m^3 and the c of the brine from 1694.2 m/sec to 1628.0 m/sec. The results of this phase with an angle β of 2.66° are compared with the results from the phase three data run at the β of 2.51° and with theory on graphs 8 and 10.

To rule out one possible source of error, a check was made to determine the flatness of the mylar interface along

the centerline of the frame in the critical region where energy transfer takes place. The conditions for the check were the same as for the previous phase. The laser set-up was moved along the centerline in 1 cm increments and β calculated. Since energy transfer started near a point 33 cm from the deep end of the frame, the check was started at 32 cm from the frame end and run to 39 cm from the frame's deep end. The resulting β's are listed in order, starting with the β at 32 cm: 2.83°, 2.98°, 2.81°, 2.97°, 3.05°, 3.12°, 3.17°, and 3.09°. There seemed to be no major bow in the mylar bottom; the change of angle with distance is, at most, +0.05 degrees/cm (becoming steeper toward the apex).

V. RESULTS

Graph 5 shows the results of the first phase of the experiment: re-establishment of the existence of the beam. The graph represents pressure amplitude as a function of depth along the centerline of the tank, at distances in both the positive and negative x-directions from the point where dumping of the first mode starts. Beginning at the right of the graph, note that the length of the tail of the exponentially decaying normal mode increases as cutoff of the second mode is approached. At the distance -5.5 cm from the start of dumping of the first mode, the transmitted beam from the second mode can be seen. The length of the exponential tail has also decreased. Then, at the point where dumping of the first mode starts (0 distance), the length of the exponential tail has increased and the beam from the second mode continues downward. Moving further to the left, it is noted that the intensity of the beam from the second mode decreases and the beam from the first mode spreads.

Graph 6 shows the results of the second phase of the experiment: determination of the beam's characteristics in the x-z plane as a function of distance from the frame centerline in the y-direction. The graph shows peak amplitude voltage as a function of θ at different r's and at different distances from the centerline of the frame. Maximum amplitude was found on the centerline and at the shortest r distance.

Amplitudes decreased with both increasing r and increasing distance off the centerline, but the decreases from one r to another r at the same distance off the centerline did not change as much as did the amplitudes between r's measured on the centerline. This is what was expected. As distance from a source increases, spreading causes a decrease in the intensity; thus the decreasing amplitude with increasing r. However, as r increases, the angle between the centerline of the main lobe of the beam (the vertex of the beam is the face of the source transducer) and the point of measurement decreases. According to line array theory, the first node of the transducer's beam should occur at 7 degrees from the centerline. As this angle is approached, the voltage amplitude decreases. At r = 10.3 cm, the centerline distance from the source is approximately 53 cm. For a distance off the centerline of 5 cm and an r = 10.3 cm, the angle to the measured point is about 5.4 degrees. If r is increased to 20 cm (source distance of 63 cm), and the centerline distance is unchanged, the angle to the measured point decreases to about 4.5 degrees. The increasing r and decreasing angle tend to keep the intensities more constant at distances away from the centerline.

Graphs 7, 8, and 9 show the results of the third phase of the experiment: determination of the dependence of the beam on the angle β. The graphs show normalized peak voltage amplitude as a function of θ at five different 4's: 10.3 cm, 15 cm, 20 cm, 25 cm, and 30 cm. Normalization was accomplished

by dividing the peak amplitude by the square root of X/r and then multiplying the quotient by a factor so that the peak experimental value and peak theoretical value would have the same magnitude. The quantity X/r is used in the theory. Therefore, the X/r values are used on the graphs. Experimental data for the five different X/r values are represented by five different symbols as listed on the graphs. The solid and dashed lines are the theoretical plots at the minimum and maximum X/r values for each set of data. These represent the theoretical envelope for each case.

The results of interest were the angular location of the maximum intensities of the beams and the general shape of the beams in relation to theoretical predictions. The angles of maximum intensity were determined in two different ways. The first method was to look at the data and take the maximum amplitude and its corresponding θ. The other method was to find the values of θ at the 6 dB down points and consider the center of the beam one-half the distance between the two θ's. Table I gives the two values for the center of the beam for selected X/r values for both the experimental and theoretical data. It should be noted that the theory, in its present state, is limited to β's no greater than about 1° for the values of θ_c and the ρ ratios used in the experiment [Ref. 3].

As β was increased from 1.52 degrees to 2.51 degrees, the angle of maximum amplitude was relatively unchanged from 15 degrees. Theory showed a change of 3 to 4 degrees. The results at $\beta = 4.41$ degrees should be noted, but their validity

is somewhat questionable due to large interference effects in the tank. The double humped pattern in graph 9 is a result of interference. From Table I, note that θ (peak) for theory and experiment are converging as β gets smaller. The percent error between the two is reducing rapidly with decreasing β.

Theoretical calculations are made, in part, by figuring the pressure amplitude at incremental distances along the boundary between the two mediums starting at the initial dumping point. It is felt that calculations made at values approaching and greater than one-half the distance from the initial dumping point to the turnaround point are not valid [Ref. 3]. A vertical arrow has been placed on the theoretical curves at the threshold of the valid data. Theoretical predictions approaching and to the right of the arrows are in question.

Graph 10 shows the results of the final phase of the experiment: determination of the dependence of the beam's characteristics on varying ρc mismatches. The graph is of the same format as the graphs in the previous phase. The same two factors, angle of maximum amplitude and shape of the beam, are again examined. Graph 10 is compared with graph 8 since the β's are very close, but the ρc of the lower layer had been changed from 0.745 kg/m^2-sec in graph 8 to 0.836 kg/m^2-sec in graph 10. Table II gives the same basic data as did Table I.

Again, the data do not correlate well with theory. There was about a 2 degree decrease from experimental data where theory predicted about a 4 degree decrease for the increase

in the ρc ratio. However, the general shape of the beams seem to follow the theory to a certain degree. As the ρc ratio increased, the beam width decreased. It must be noted that the sharp decrease in theoretical beam width is attributed mainly to data in a questionable area to the right of one of the arrows. Again, there were some reflections that could not be removed that could have affected the data of graph 10.

VI. CONCLUSIONS

Results of this experiment show that, when a tapered fluid layer excited with normal modes overlies a fluid layer with a higher ρc, a beam is formed in the lower layer. Energy begins to be transferred into the lower layer at the point where the depth of the tapered layer is equal to a cutoff depth for a normal mode.

The characteristics of the beam in the lower layer are directly affected by the beam pattern of the source transducer. Very little energy is transferred into the lower layer in regions where the source beam is nulled.

There is good agreement between theory in its present state and experimental data for values of θ which are less than the θ where maximum pressure amplitude is reached. However, the location of the maximum amplitude of the beam and pressure amplitudes at values of θ larger than θ of maximum amplitude cannot be predicted accurately with the theory. In general, theory and experiment are in fair qualitative agreement, both displaying similar beam shapes and both show the beam maximum shifting in the same direction when β and the ρc ratio are changed. The differences between theoretical predictions and experimental results are not surprising for two reasons: 1) experimental difficulties associated with interference at large values of θ, and 2) the fact that for the parameters used in the experiment, the theory is restricted to angles of β no larger than about 1°.

WAVE PROPAGATION IN A WEDGE

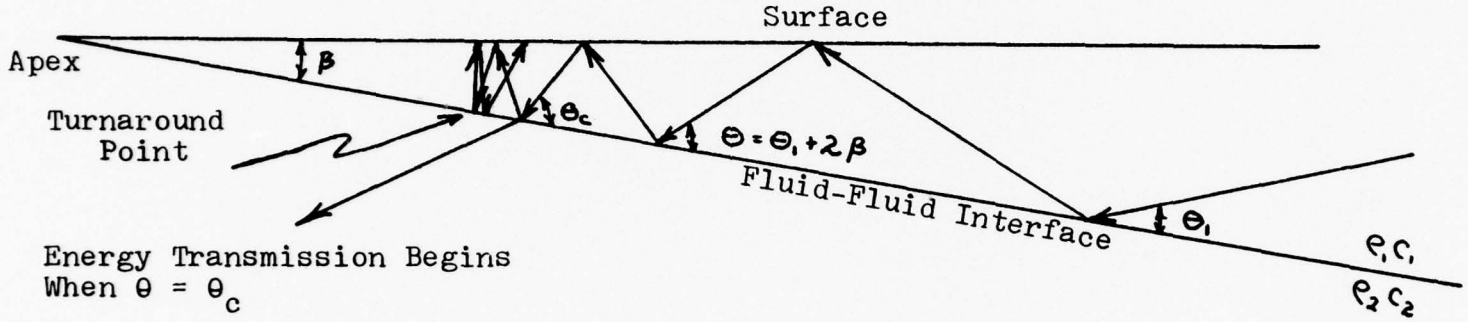

Figure 1

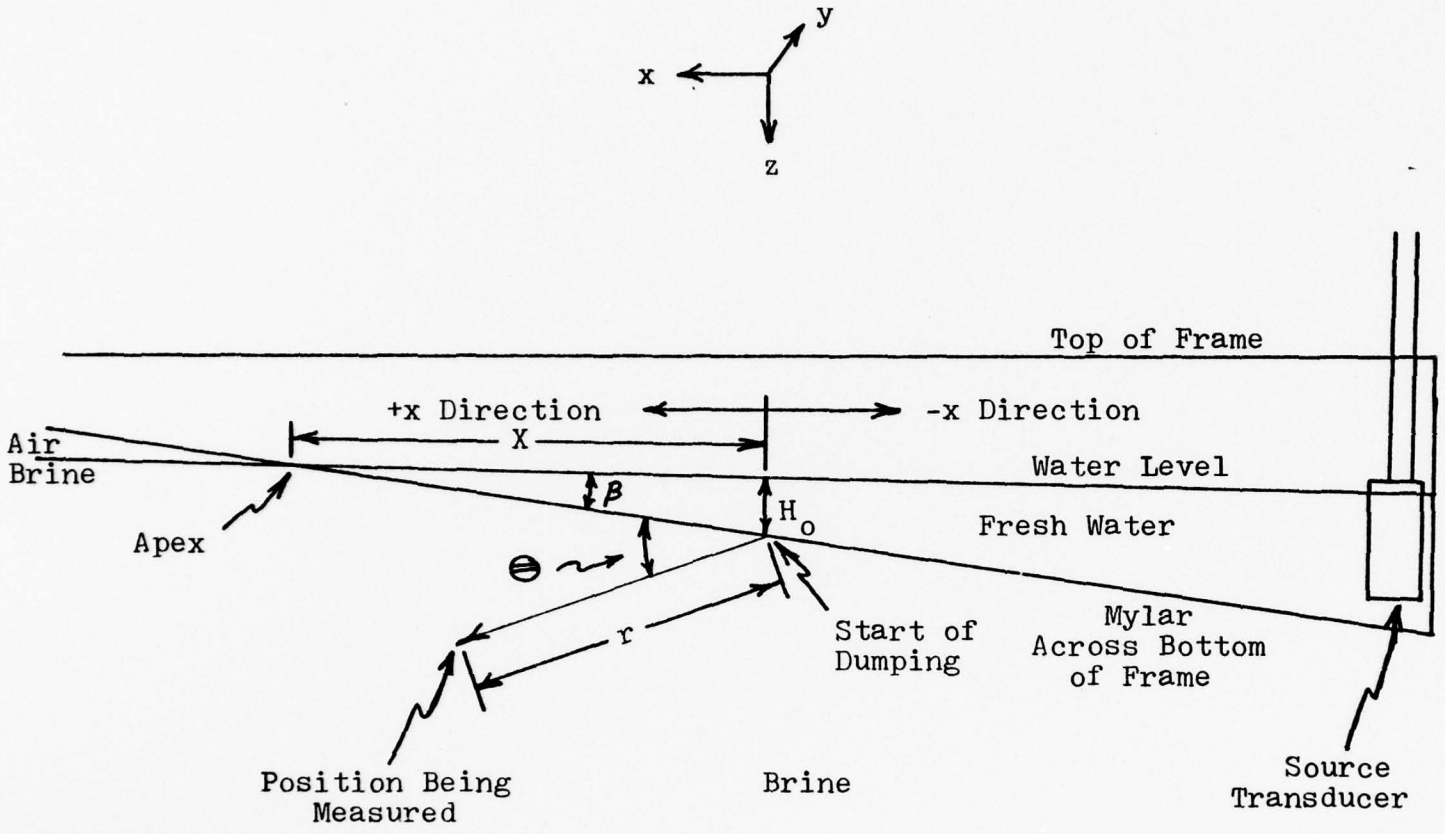
y
x
z
Top of Frame
+x Direction
-x Direction
X
Air
Brine
Water Level
β
H_o
Fresh Water
Apex
θ
r
Start of
Dumping
Mylar
Across Bottom
of Frame
Position Being
Measured
Brine
Source
Transducer

Figure 2

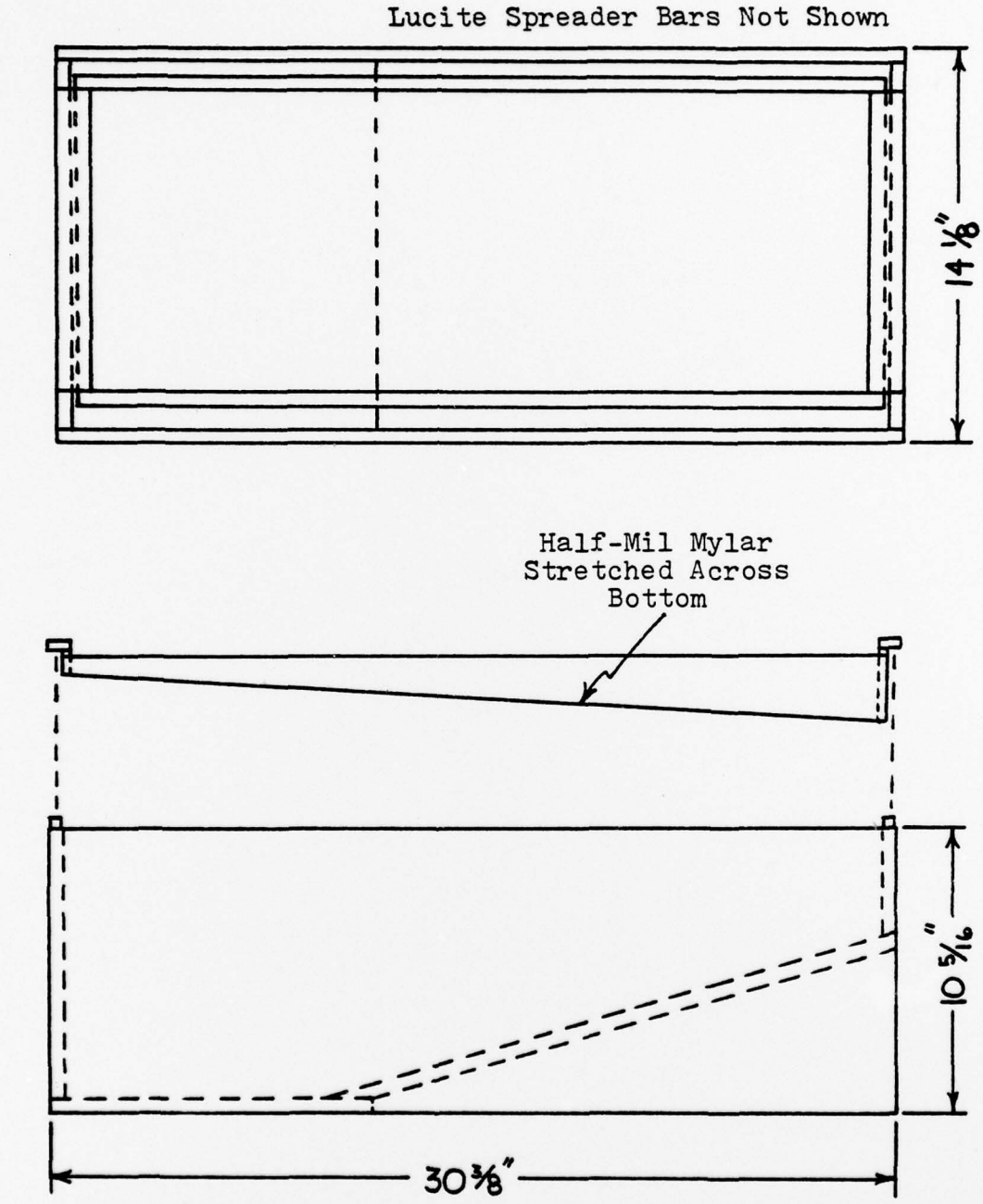

Scale 1": 6"

Tank and Frame

Figure 3

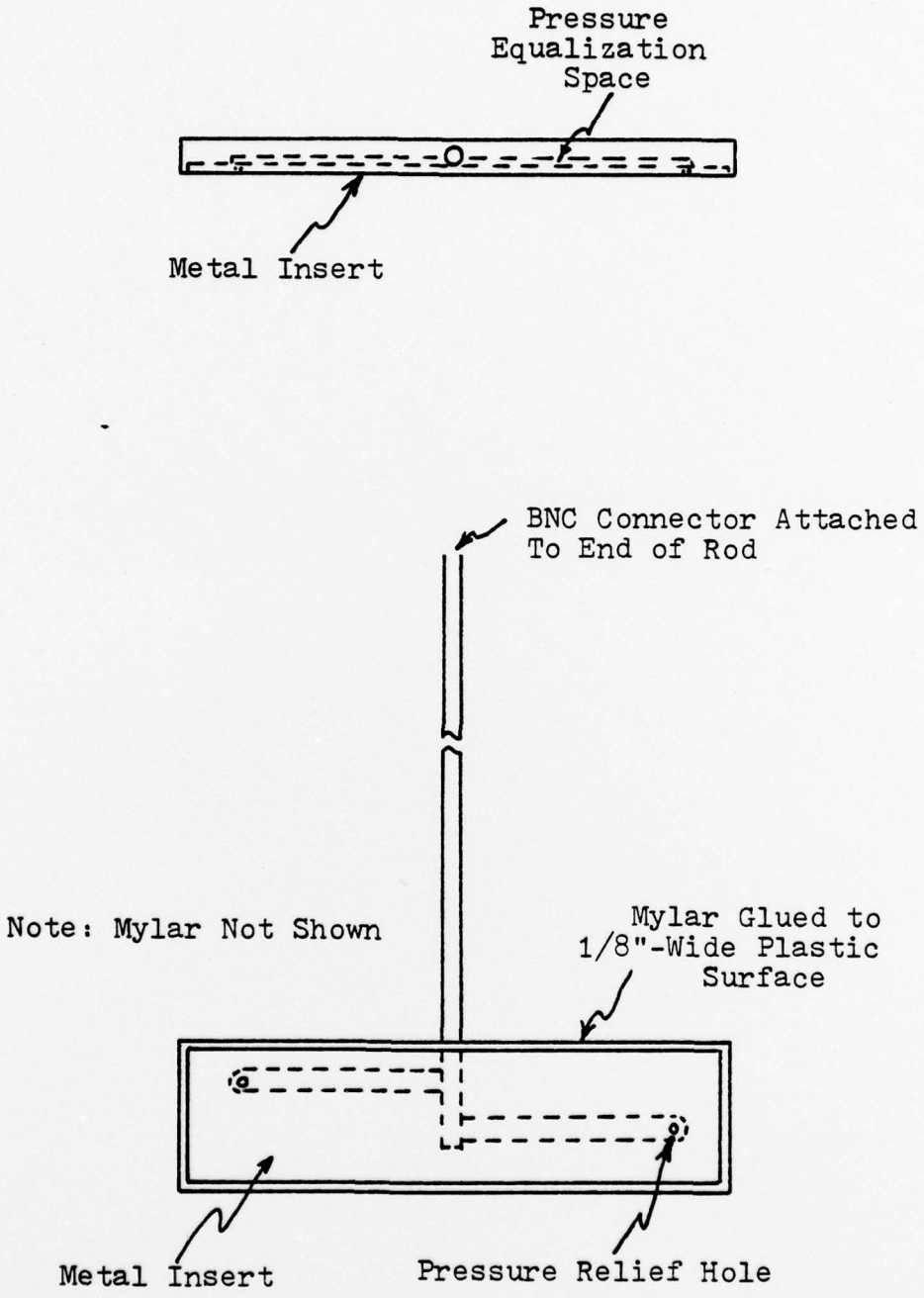

Mylar Source Transducer

Figure 4

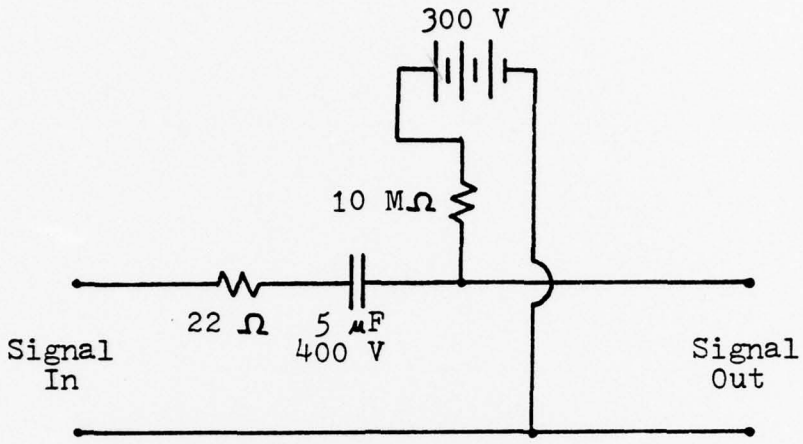

DC Biasing Network

Figure 5

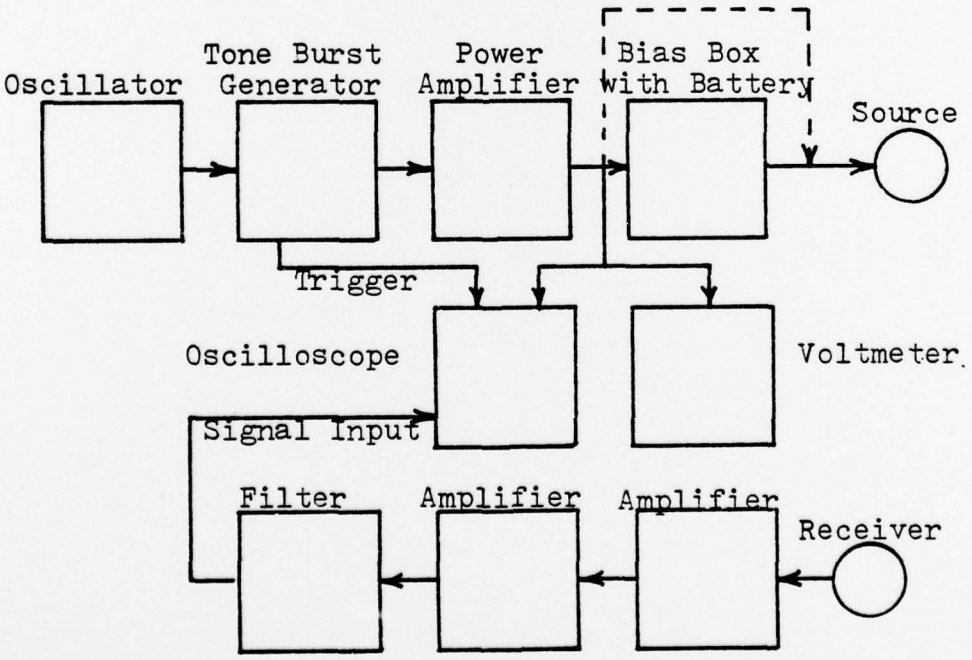

Electrical Set Up

Figure 6

APPENDIX B

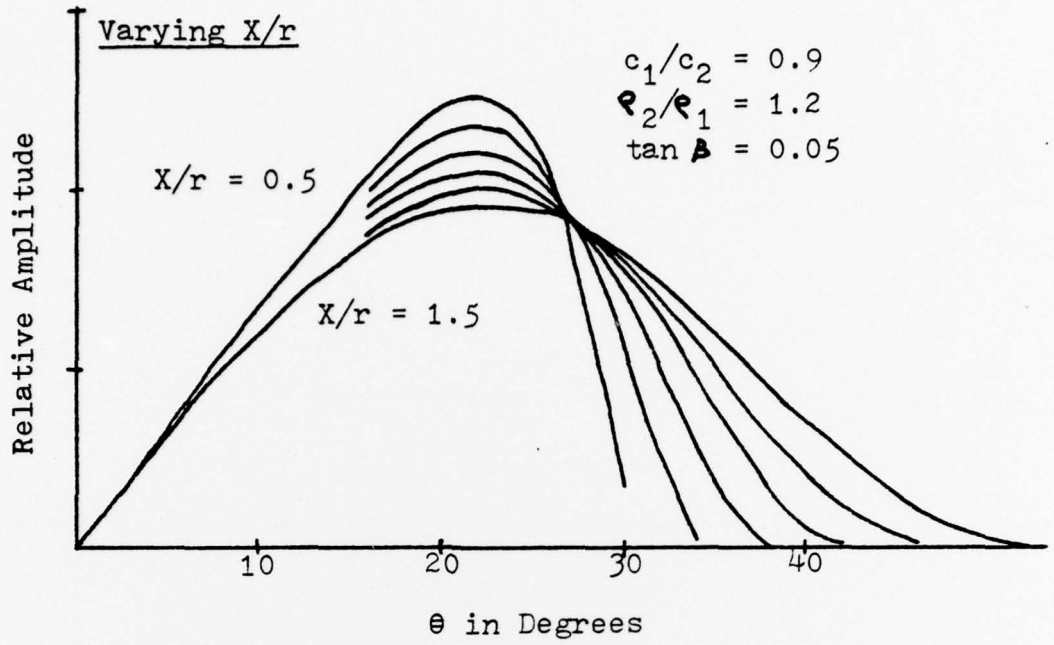

Graph 1

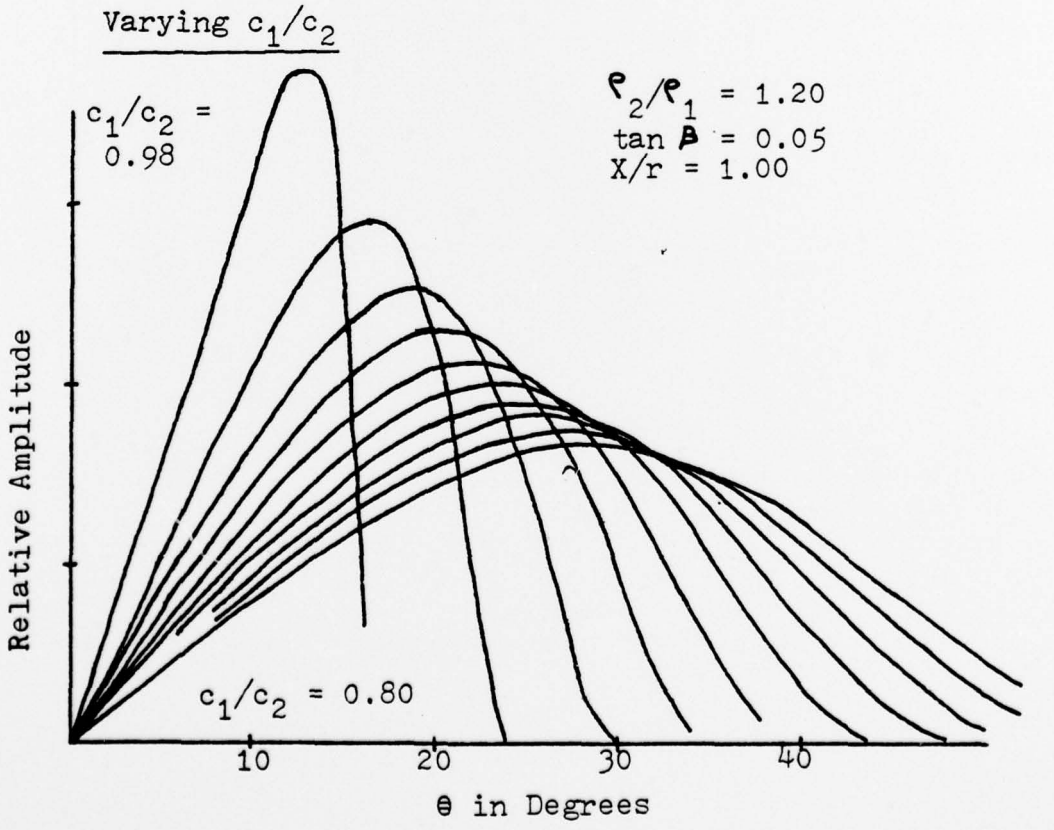

Graph 2

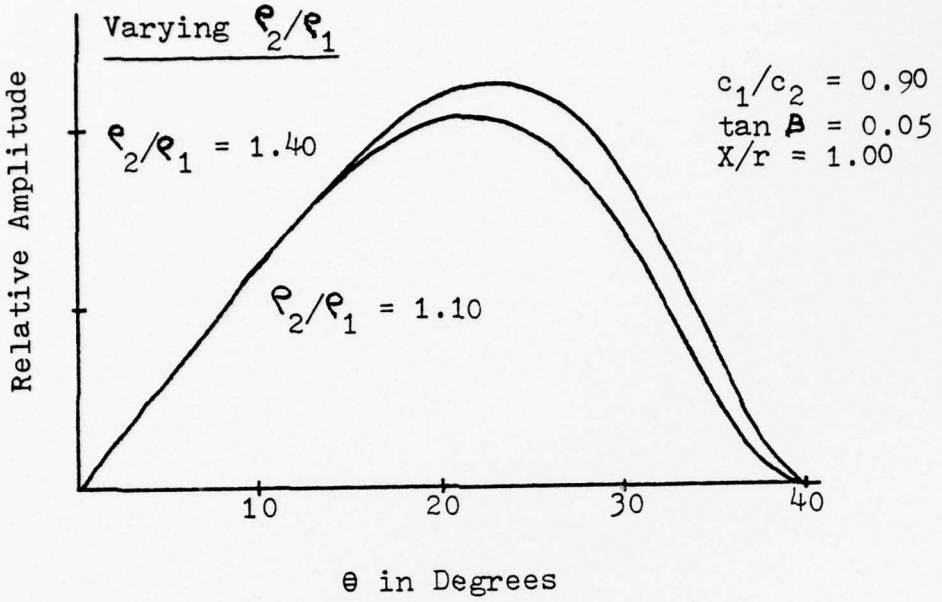

Graph 3

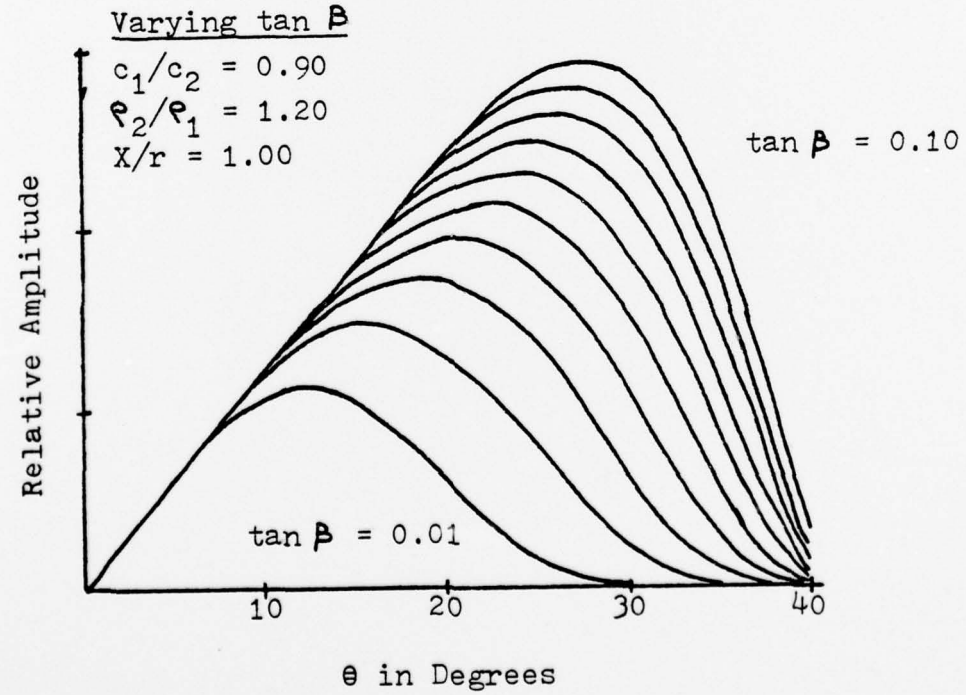

Graph 4

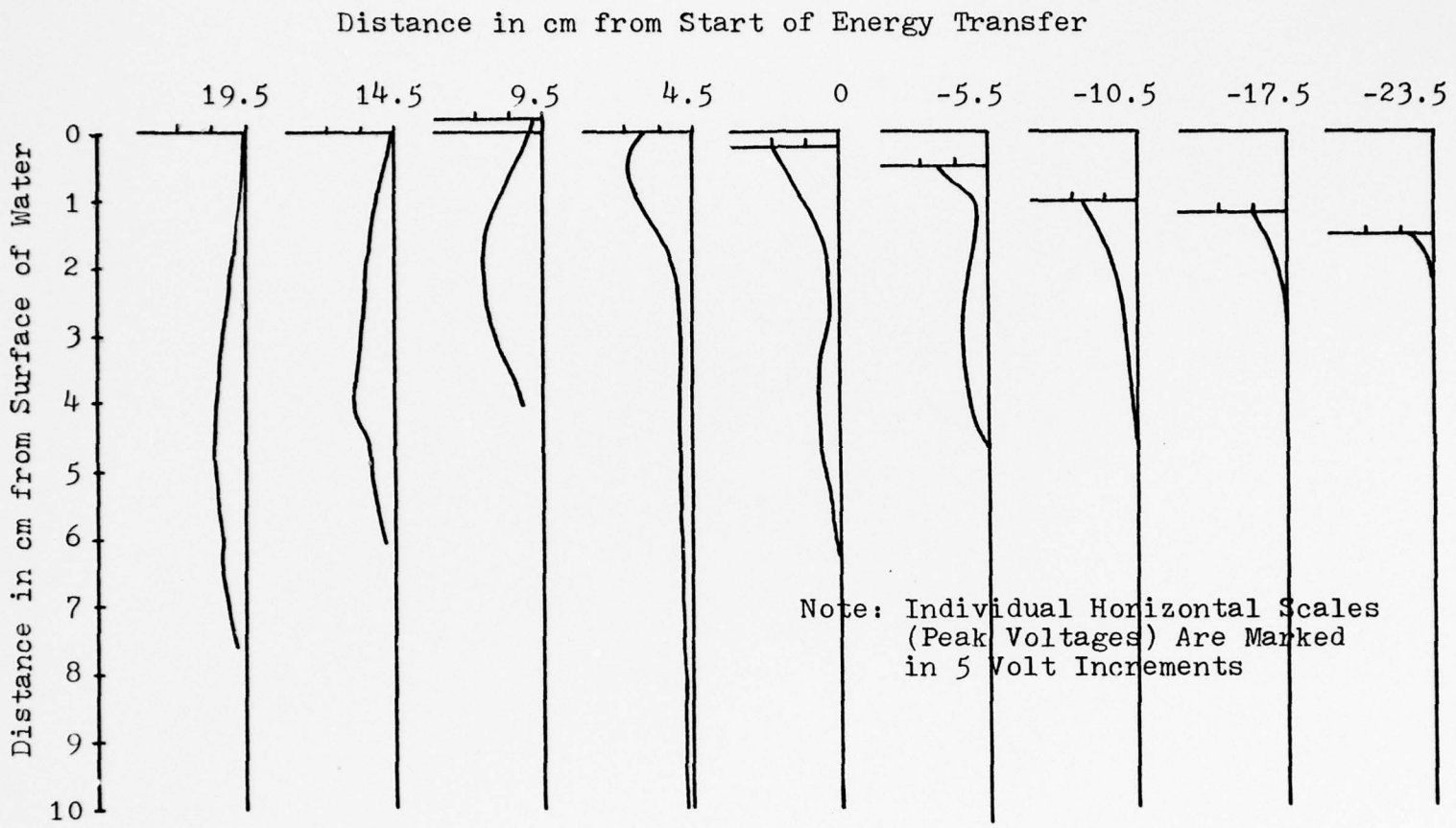
Distance in cm from Start of Energy Transfer
19.5
14.5
9.5
4.5
0
-5.5
-10.5
-17.5
-23.5
Distance in cm from Surface of Water
0
1
2
3
4
5
6
7
8
9
10
Note: Individual Horizontal Scales
(Peak Voltages) Are Marked
in 5 Volt Increments

Graph 5

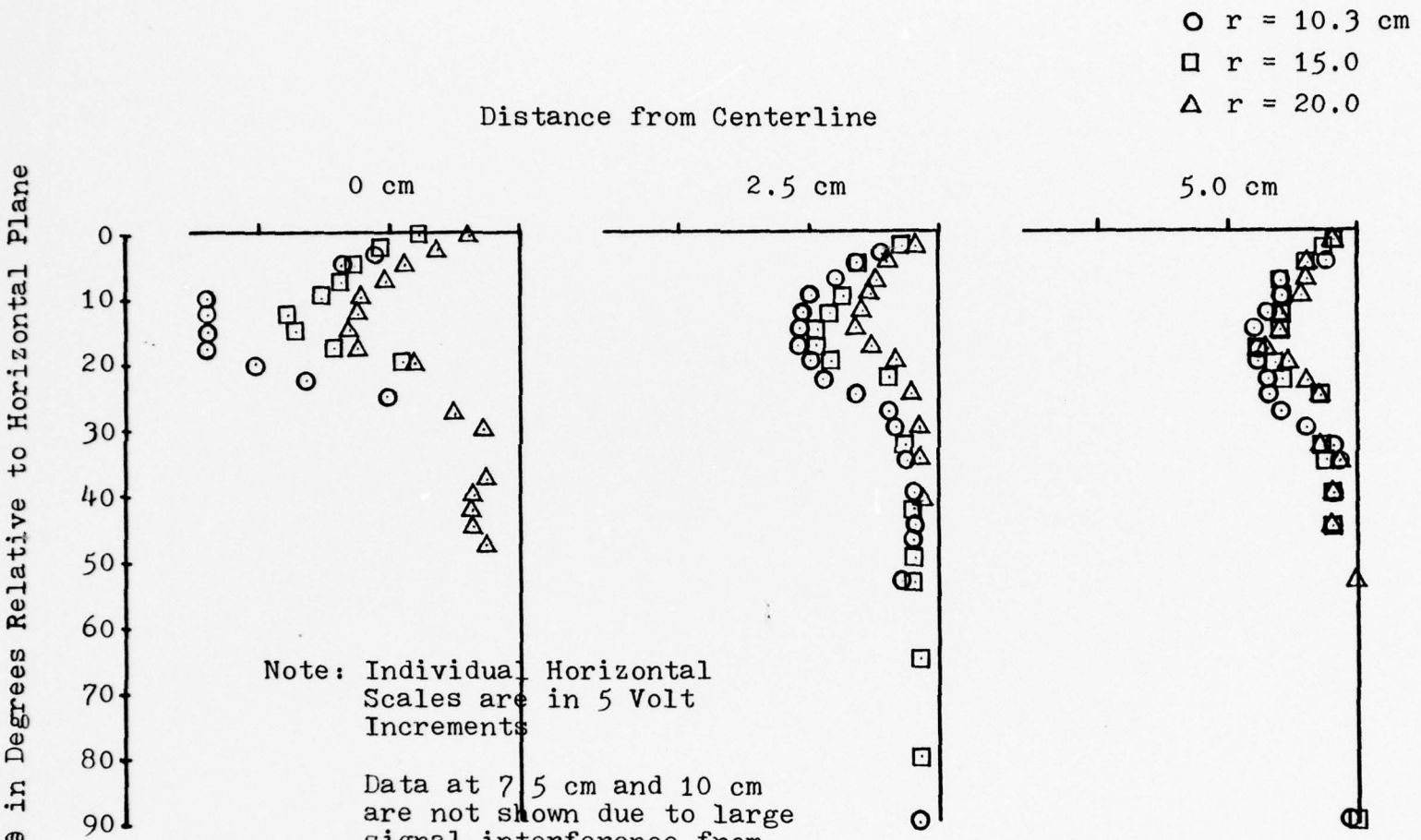
○ r = 10.3 cm
□ r = 15.0
△ r = 20.0
Distance from Centerline
0 cm
2.5 cm
5.0 cm
θ in Degrees Relative to Horizontal Plane
0
10
20
30
40
50
60
70
80
90
Note: Individual Horizontal Scales are in 5 Volt Increments
Data at 7.5 cm and 10 cm are not shown due to large signal interference from the tank sides.

Graph 6

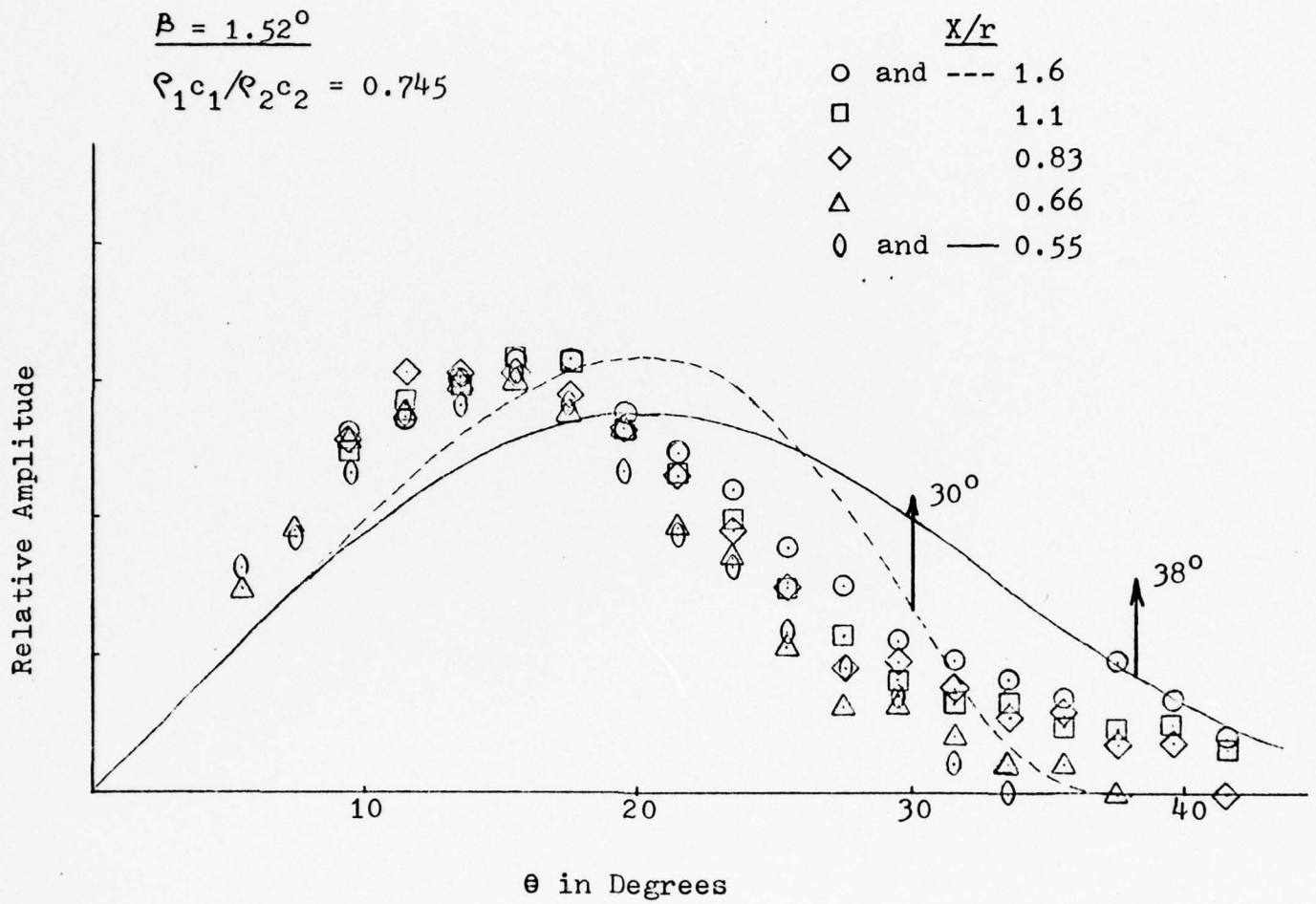
β = 1.52°
ρ1c1/ρ2c2 = 0.745
X/r
○ and --- 1.6
□ 1.1
◇ 0.83
△ 0.66
◊ and —— 0.55
Relative Amplitude
30°
38°
10
20
30
40
θ in Degrees

Graph 7

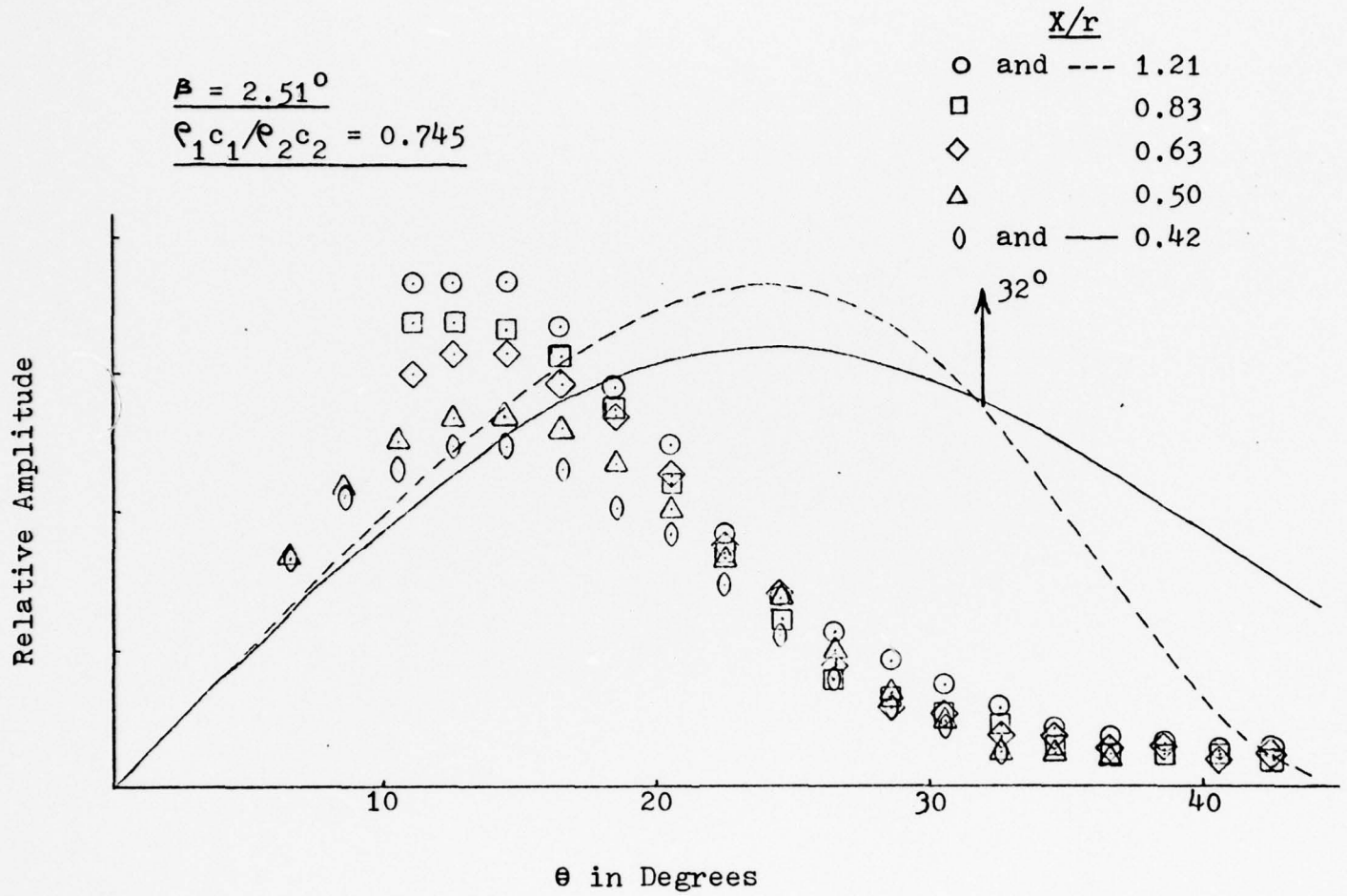
β = 2.51°
ρ1c1/ρ2c2 = 0.745
X/r
○ and --- 1.21
□ 0.83
◇ 0.63
△ 0.50
◊ and —— 0.42
32°
Relative Amplitude
10
20
30
40
θ in Degrees

Graph 8

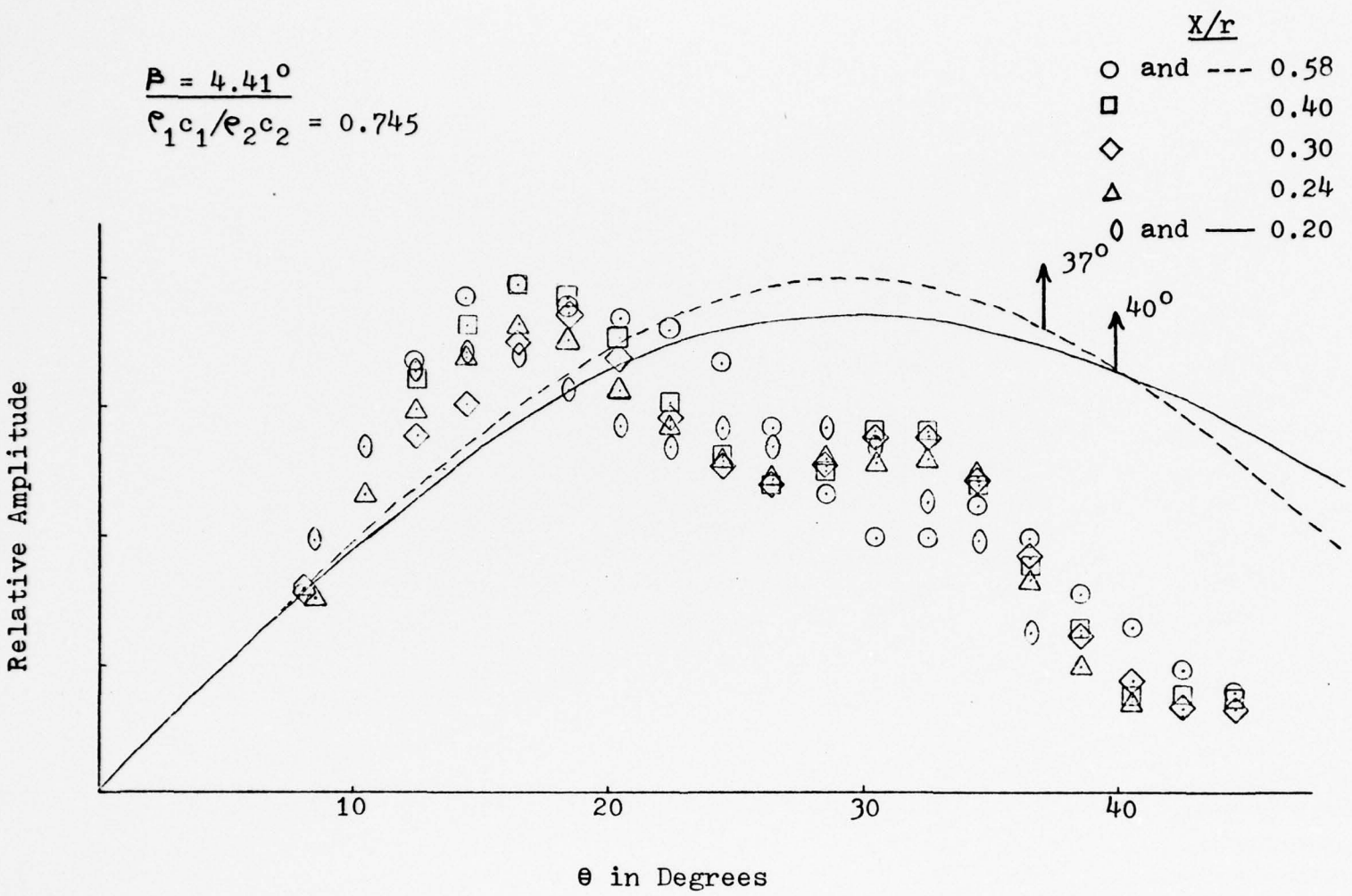
β = 4.41°
ρ1c1/ρ2c2 = 0.745
X/r
○ and --- 0.58
□ 0.40
◇ 0.30
△ 0.24
◊ and —— 0.20
37°
40°
Relative Amplitude
10
20
30
40
θ in Degrees

Graph 9

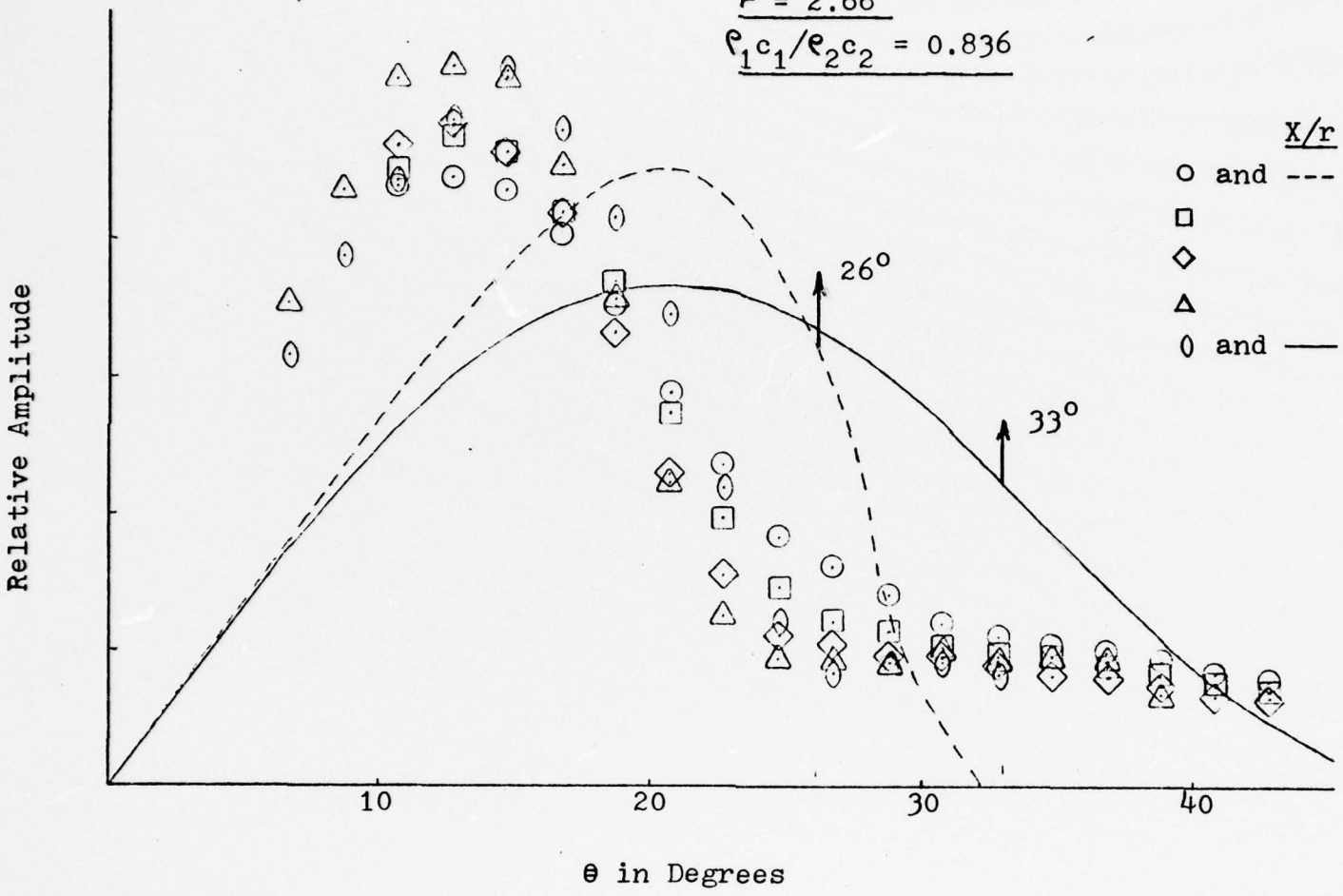
β = 2.66°
ρ1c1/ρ2c2 = 0.836
X/r
○ and --- 1.31
□ 0.90
◇ 0.68
△ 0.54
◊ and —— 0.45
26°
33°
Relative Amplitude
10
20
30
40
θ in Degrees

Graph 10

APPENDIX C

β°	$\frac{(\rho c)_1}{(\rho c)_2}$	X/r	θ			
			Experimental		Theoretical	
			Act. Peak	6 dB Mid Point	Act. Peak	6 dB Mid Point
1.52	0.745	0.55	15.5	15	20	20.75
		0.66	13.5	15		
2.51	0.745	0.41	14.0	14.38	24	22.38
		0.50	13.3	15.5		
4.41	0.745	0.20	20	21	30	29.5
		0.24	16.4	22.5		

Table I

β°	$\frac{(\rho c)_1}{(\rho c)_2}$	X/r	θ			
			Experimental		Theoretical	
			Act. Peak	6 dB Mid Point	Act. Peak	6 dB Mid Point
2.51	0.745	0.41	14	14.38	24	22.38
		0.50	13.3	15.5		
2.66	0.836	0.45	14.7	13.5	20	17.63
		0.54	12.67	12.88		

Table II

BIBLIOGRAPHY

1. Edwards, J.N., Jr., A Preliminary Investigation of Acoustic Energy Transmission from a Tapered Fluid Layer into a Fast Bottom, M.S. Thesis, Naval Postgraduate School, Monterey, 1976.

2. Coppens, A.B., and Sanders, J.V., Acoustics, Part III, p. 261-281, material used in Underwater Acoustics Class, Naval Postgraduate School, Monterey, California, 1977.

3. Personal communications with A.B. Coppens, Code 61 Cz, Department of Physics and Chemistry, Naval Postgraduate School, Monterey, California, November 1977.

INITIAL DISTRIBUTION LIST

		No. Copies
1.	Defense Documentation Center Cameron Station Alexandria, Virginia 22314	2
2.	Library, Code 0212 Naval Postgraduate School Monterey, California 93940	2
3.	Department Chairman, Code 61 Department of Physics and Chemistry Naval Postgraduate School Monterey, California 93940	2
4.	Assoc. Professor J. V. Sanders, Code 61 Sd Department of Physics and Chemistry Naval Postgraduate School Monterey, California 93940	1
5.	Assoc. Professor A. B. Coppens, Code 61 Cz Department of Physics and Chemistry Naval Postgraduate School Monterey, California 93940	1
6.	Dr. P. H. Moose, Code 61 Me Department of Physics and Chemistry Naval Postgraduate School Monterey, California 93940	1
7.	LT Gregory B. Netzorg, U.S.N. 1818 Loyola Court Chula Vista, California 92010	1
8.	Dr. E. P. Cooper, Code 013 Naval Ocean Systems Center San Diego, California 92152	2